The Emergence of the Spatial Structure of Tectal Spontaneous Activity Is Independent of Visual Inputs

Thomas Pietri, Sebastián Alejo Romano, Veronica Pérez-Schuster, Jonathan Boulanger-Weill, Virginie Candat, German Sumbre

Cell Reports

Report

The Emergence of the Spatial Structure of Tectal Spontaneous Activity Is Independent of Visual Inputs

Graphical Abstract

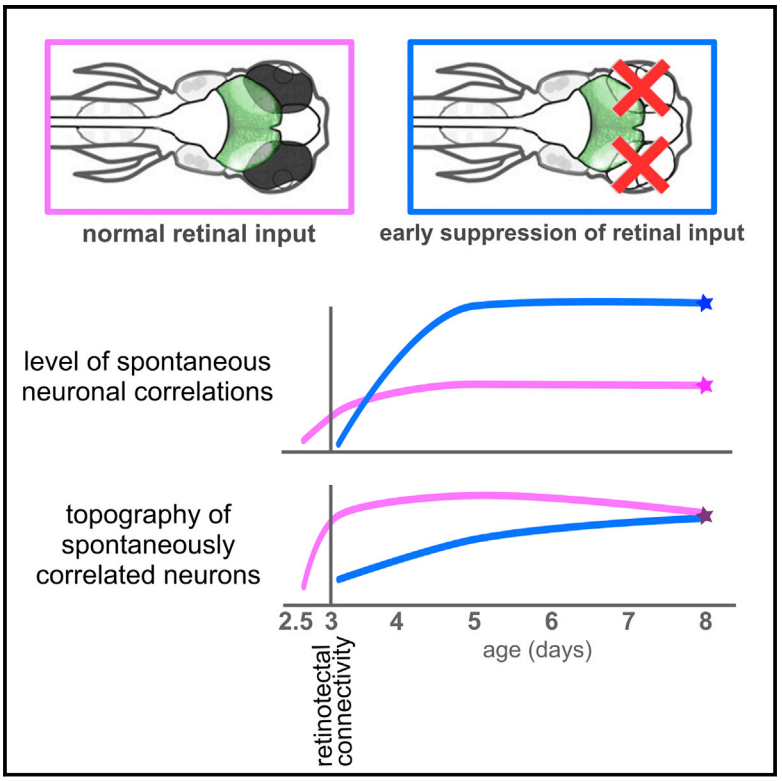

Authors

Thomas Pietri, Sebastián A. Romano, Verónica Pérez-Schuster, Jonathan Boulanger-Weill, Virginie Candat, Germán Sumbre

Correspondence

sumbre@biologie.ens.fr

In Brief

The influence of retinal inputs on the development of the spontaneous neuronal activity of the tectal circuit is unknown. Pietri et al. show that retinal inputs are dispensable for the development of the spatial structure of spontaneous tectal activity, suggesting that the tectal circuit is preconfigured for its functional role.

Highlights

- Development of tectal circuitry is influenced by the onset of retinal inputs
- Enucleations impact the development of the tectum's spontaneous activity correlations
- Enucleations only delay the topography of the correlated activity
- In the absence of retinal inputs, the tectal circuitry is capable of predicting behavior

Pietri et al., 2017, Cell Reports *19*, 939–948
May 2, 2017
http://dx.doi.org/10.1016/j.celrep.2017.04.015

CellPress

Cell Reports
Report

The Emergence of the Spatial Structure of Tectal Spontaneous Activity Is Independent of Visual Inputs

Thomas Pietri,[1,2] Sebastián A. Romano,[1,3] Verónica Pérez-Schuster,[1,4] Jonathan Boulanger-Weill,[1] Virginie Candat,[1] and Germán Sumbre[1,5,*]

[1]IBENS, Département de Biologie, Ecole Normale Supérieure, CNRS, Inserm, PSL Research University, 75005 Paris, France
[2]Present address: Biological Sciences, New Jersey Institute of Technology, Newark, NJ 07102, USA
[3]Present address: Instituto de Investigación en Biomedicina de Buenos Aires (IBioBA) – CONICET – Partner Institute of the Max Planck Society, Buenos Aires C1425FQD, Argentina
[4]Present address: Laboratorio de Neurobiología de la Memoria, Departamento Fisiología, Biología Molecular y Celular and Departamento de Física, UBA, Buenos Aires C1428EG, Argentina
[5]Lead Contact
*Correspondence: sumbre@biologie.ens.fr
http://dx.doi.org/10.1016/j.celrep.2017.04.015

SUMMARY

The brain is spontaneously active, even in the absence of sensory stimulation. The functionally mature zebrafish optic tectum shows spontaneous activity patterns reflecting a functional connectivity adapted for the circuit's functional role and predictive of behavior. However, neither the emergence of these patterns during development nor the role of retinal inputs in their maturation has been characterized. Using two-photon calcium imaging, we analyzed spontaneous activity in intact and enucleated zebrafish larvae throughout tectum development. At the onset of retinotectal connections, intact larvae showed major changes in the spatiotemporal structure of spontaneous activity. Although the absence of retinal inputs had a significant impact on the development of the temporal structure, the tectum was still capable of developing a spatial structure associated with the circuit's functional roles and predictive of behavior. We conclude that neither visual experience nor intrinsic retinal activity is essential for the emergence of a spatially structured functional circuit.

INTRODUCTION

Sensory brain areas are continuously active, even in the absence of external stimulation. This ongoing spontaneous activity, defined as the intrinsic brain activity not driven by sensory stimuli, was once considered to be independent biophysical noise and thought to interfere with brain computations (Faisal et al., 2008; Tolhurst et al., 1983). This view has changed in recent years, as spontaneous activity has been found to be structured in space and time (Fiser et al., 2004; Jetti et al., 2014; Kenet et al., 2003; Kirkby et al., 2013; Romano et al., 2015; Smith and Kohn, 2008). In sensory brain areas, spontaneous activity can exhibit spatial patterns that match functional sensory maps (Jetti et al., 2014; Kenet et al., 2003; Romano et al., 2015).

Across the different sensory modalities, the visual system is the most extensively investigated. Although the initial organization of the retinorecipient brain areas is coarsely established by molecular cues (Triplett, 2014), activity-dependent mechanisms are thought to be essential for their maturation (Huberman et al., 2008). In the developing optic tectum, visual conditioning can alter neuronal functional properties, such as the formation of neuronal receptive fields (Vislay-Meltzer et al., 2006; Zhou et al., 2003) and the development of intratectal connectivity (Pratt et al., 2008). Furthermore, it causes short-term changes in spontaneous circuit dynamics (Sumbre et al., 2008). On the other hand, impeding visual experience by dark-rearing zebrafish larvae hardly alters their visual tectal response properties (Niell and Smith, 2005). Yet, in the tectum of dark-reared *Xenopus* tadpoles, temporal correlations between neurons and the reliability of their responses to a visual stimulus are significantly reduced (Xu et al., 2011). Besides visual experience, the retinorecipient circuits can also be influenced by the intrinsic activity of the retina (Ackman and Crair, 2014). Several studies have shown the crucial role of intrinsic retinal activity on the proper organization of retinal ganglion cell (RGC) projections within their target circuits (formation of retinotopic and eye-segregation maps; Kirkby et al., 2013; Kita et al., 2015). However, only a few have examined the effect of the retina on the maturation of the spontaneous activity of retinorecipient circuits. Specifically, optic nerve transection, or disruption of retinal waves (in the β2-nAChR mouse knockout) before eye opening, induced an increase of the spontaneous activity in the dorsal lateral geniculate nucleus of ferrets (Weliky and Katz, 1999) and in the superior colliculus (SC) of mice (Burbridge et al., 2014).

Despite these advances, a comprehensive study on the development of the spontaneous activity of retinorecipient areas, and on the influence of retinal activity on this process, is still lacking. To that end, we examined the single-neuron and circuit developmental dynamics of the spontaneous activity of the optic tectum

of intact, non-anesthetized, non-paralyzed, behaving zebrafish larvae throughout the main period of its functional maturation. These results were then compared to those from enucleated larvae whose tecta never received retinal inputs.

The optic tectum of the zebrafish, homologous to the mammalian SC, is involved in spatial vision detection (e.g., detection of prey) and generation of orienting motor commands (Gahtan et al., 2005; Krauzlis et al., 2013). In the functionally mature tectal circuit, ongoing spontaneous activity is organized in assemblies composed of highly correlated neurons. These neuronal assemblies are spatially organized reflecting the functional retinotopic map, they are tuned to biologically relevant visual stimuli (e.g., prey), and their activation predicted orienting tail movements. This suggests that the tectal circuitry is adapted for its functional role (Romano et al., 2015).

In the present study, we observed that the development of the spatiotemporal structure of spontaneous activity markedly changed at the onset of retinotectal connections, at 3 days post-fertilization (dpf; Niell and Smith, 2005; Stuermer, 1988). In retina-deprived conditions, the development of a spatiotemporal structure was delayed. By 8 dpf, when the tectal circuitry is functionally mature (Niell and Smith, 2005; Romano et al., 2015), the temporal structure (correlation level of neuronal activities) remained strongly impacted by retinal-input deprivation, yet the spatial structure (the topography of neuronal assemblies) reached similar values to those of intact larvae. Moreover, the deprived tectal circuit appeared functional, as the spontaneous activation of its tectal assemblies was still predictive of self-generated motor behaviors.

RESULTS

Development of Tectal Neurons' Spontaneous Activity

To study the maturation of the intrinsic network dynamics of the optic tectum, we monitored the spontaneous activity of transgenic zebrafish larvae expressing pan-neuronally the genetically encoded calcium indicator GCaMP3 (Tian et al., 2009), using two-photon scanning microscopy. This technique enables monitoring of the spontaneous dynamics of a significant portion of the optic tectum (893 ± 14 neurons from 135 larvae) at different developmental stages, in the presence (66–70, 74–80, 122–128, and 193–199 hr post-fertilization, hereinafter referred to in the text as 2.5, 3, 5, and 8 dpf) or absence (3, 5, and 8 dpf) of the main tectal sensory input, the retinal afferents (Figure 1A).

We first examined different properties of single tectal neurons: the average frequency of the Ca^{2+} transients (Figure 1B), their duration (Figure 1C), and their amplitude (ΔF/F; Figure 1D). In intact 2.5-dpf larvae, 7.63% ± 2.27% of the neurons did not show significant Ca^{2+} transients during the 1-hr recording period (silent neurons). At all other developmental stages, less than 0.22% ± 0.07% of the neurons were silent. The average frequency of neuronal Ca^{2+} events showed a progressive increase during development of the intact larvae (Figure 1B). In contrast, between 2.5 and 3 dpf, the period at which the retina establishes a functional connection with the optic tectum (functional synaptic connectivity; Niell and Smith, 2005), abrupt changes occurred in the duration (decrease from 2.5 to 3 dpf, $p = 5.10^{-4}$; Figure 1C) and the amplitude (increase, $p < 10^{-4}$; Figure 1D) of the Ca^{2+} events. The developmental dynamics of the frequency, duration, and amplitude of the Ca^{2+} events were remarkably different in larvae enucleated at 2 dpf (before the retina creates functional connections with the optic tectum). Their frequency sharply increased at 8 dpf (0.054 Hz versus 0.015 Hz in intact 8-dpf larvae; $p < 10^{-4}$). In contrast, their duration at 3 and 5 dpf remained similar to that of 2.5-dpf intact larvae ($p > 0.39$ and $p > 0.61$, respectively) but decreased to a level similar to that of intact larvae by 8 dpf ($p > 0.27$). Throughout maturation, we observed a constant increase in the frequency of spontaneous synchronous Ca^{2+} events (synchronous events were defined as periods in which at least 10% of the imaged tectal neurons were active at a given imaged frame). In enucleated larvae, this increase was significantly larger than in intact ones. Although the frequency of synchronous events at 3 dpf was not significantly different from that of intact larvae at 2.5 dpf ($p > 0.66$), we observed a large increase at 5 and 8 dpf ($p < 10^{-4}$; Figure 1E).

Overall, these results suggest that, at the onset of retinotectal interactions, the new excitatory retinal inputs strongly influence the maturation of the tectal neurons, while their absence creates a long-lasting profound plasticity effect (Keck et al., 2013). The differences in the duration and the amplitude of the spontaneous Ca^{2+}-events caused by the enucleations suggest that retinal inputs play an important role in the early physiological maturation of the tectal neurons (Sheroziya et al., 2009; Warp et al., 2012). In addition, the development of large synchronous events in the course of tectal maturation also suggests that the spontaneous tectal activity is temporally structured.

Development of Spontaneous Activity Neuronal Pairwise Correlations

To evaluate the putative temporal structure of the spontaneous activity in the optic tectum and its development, we first computed the neuron pairwise spontaneous activity Pearson's correlation coefficients at each developmental stage in intact and enucleated larvae (Figures S1A and S1B). Since we observed dramatically different levels of overall activity in the different conditions, we assessed the significance of these correlations by computing the Jensen-Shannon distance (JSD) between the distributions of correlations found in the measured and time-shuffled calcium activities (Figure 1F; JSD is a measurement of the difference between two distributions: here, it increases with the significance of the measured correlations). In intact animals, the average JSD progressively increased from stage to stage across development. In contrast, enucleated larvae showed a significantly larger average JSD value at 5 dpf than at 3 dpf ($p < 10^{-5}$); the latter was closer to the average JSD of 2.5-dpf intact larvae than to that of 3-dpf intact larvae. In addition, this temporal structure mostly reflected correlations within each tectal hemisphere in both intact and enucleated larvae (Figures S1C and S1D). However, a few high-correlation values were also observed between neuronal pairs across tectal hemispheres, reflecting the existence of specific functional connections between both hemispheres, either directly through the intertectal commissure or indirectly via other relay nuclei (Nevin et al., 2010). The lack of retinal inputs equally affected the development of intra- and intertectal correlations. Since the retina only projects to the contralateral tectum (Burrill and Easter, 1994), the

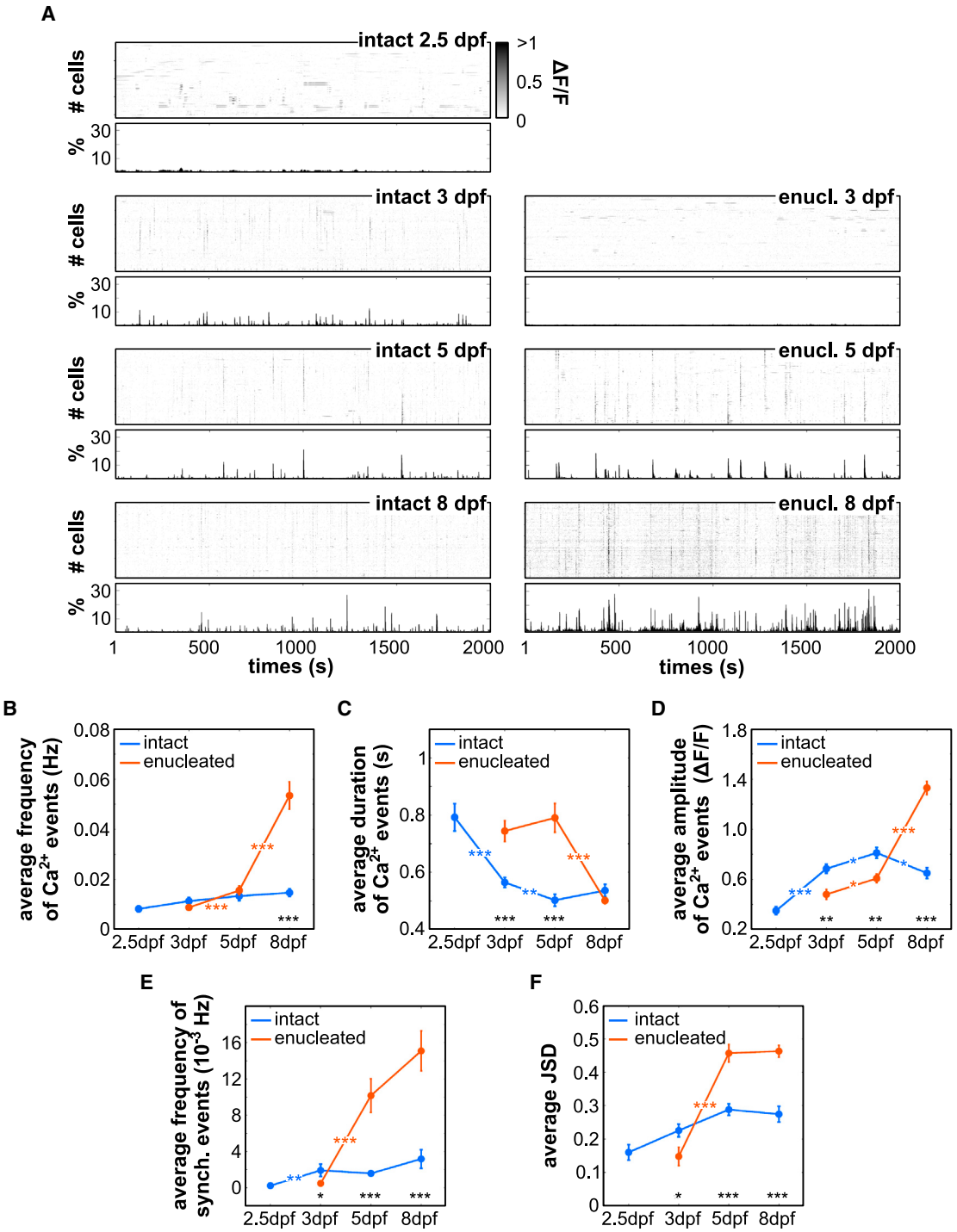

Figure 1. Maturation of the Spontaneous Tectal Activity in Intact and Retinal Input Deprived Larvae

(A) Raster plot examples of the spontaneous significant Ca^{2+} events of intact larvae at 2.5, 3, 5, and 8 dpf (left column, ns = 880, 1,012, 927 and 810 neurons, respectively) and an enucleated larva at 3, 5, and 8 dpf (right column, ns = 980, 882, and 879 neurons, respectively). The rasters represent a period of 2,000 s out of ~1 hr of recording sessions. Gray scale: amplitude of the Ca^{2+} events. The percentage of active neurons at each time point is represented below each raster plot.

(B–D) Developmental dynamics of the average frequency (B), duration (C), and relative fluorescence variation (D; ΔF/F) of the spontaneous Ca^{2+} events.

(E) Average frequency of the synchronous spontaneous Ca^{2+} events.

(F) Average distance between the distributions of the pairwise correlation coefficients and their respective random surrogate versions for each developmental stage in intact and enucleated larvae, quantified as JSD. Blue indicates intact larvae, and red indicates enucleated larvae.

*: $p < 0.05$; **: $p < 0.01$; ***: $p < 0.001$. Error bars indicate SEM.

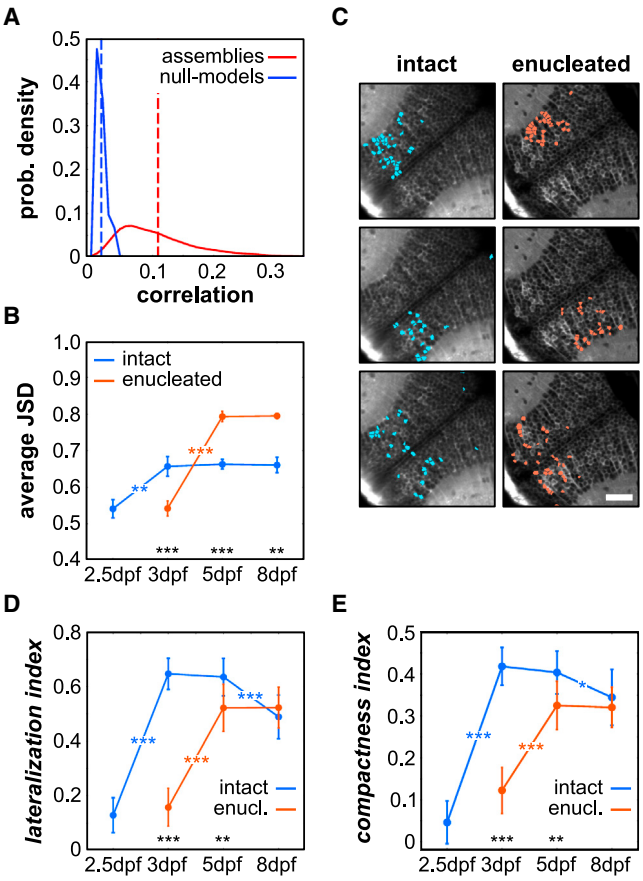

Figure 2. The Tectal Spontaneous Activity Structure Is Organized in Functional Neuronal Assemblies

(A) Probability (prob.) density of the distributions of the average correlations between neurons within each assembly and the corresponding null model, in intact larvae 5 dpf. The dotted lines represent the average correlation, in red for the data (0.108 ± 0.010) and blue for the null models (0.016 ± 0.002).

(B) Average JSD for the spontaneous neuronal assemblies across the different developmental stages, in intact and enucleated conditions.

(C) Topographies of representative neuronal assemblies emerging from the spontaneous activity of a 5 dpf intact and enucleated larva. Scale bar, 100 μm.

(D and E) Average index of lateralization, depicting the position of neurons within an assembly across both tecta (D), and index of compactness, representing the dispersion of neurons within a given assembly (E), for the neuronal assemblies during development, in intact and enucleated (enucl.) larvae.

Blue indicates intact larvae, and red indicates enucleated larvae in (B), (D), and (E).

*: $p < 0.05$; **: $p < 0.01$; ***: $p < 0.001$. Error bars indicate SEM.

latter observation indicates that common retinal inputs alone cannot explain the observed developmental changes. Overall, these results suggest an important strengthening of the overall connectivity in the tectal network after the formation of retinotectal connections.

Spontaneous Tectal Activity Is Organized into Neuronal Assemblies, even in the Absence of Retinal Inputs

Having demonstrated the establishment of significant temporal correlations among tectal neurons, we then asked whether these correlated neurons displayed a specific topographic organization (spatial structure). For this purpose, we used a recently developed method based on dimensionality reduction (principal-component analysis) and factor analysis for data clustering, which allowed the extraction of neuronal assemblies composed of highly correlated neurons while allowing for overlap between the neuronal assemblies (so that neurons could belong to different assemblies at different time points; Figures 2A and 2B). The number of assemblies, as well as the number of neurons per assembly, largely evolved during development (Figures S2A and S2B). While the average number of assemblies in enucleated larvae was mostly smaller across developmental stages when compared to intact larvae, they showed similar developmental dynamics (Figure S2A). The average number of neurons per neuronal assembly of enucleated larvae reached the same level as that of intact ones by 8 dpf ($p = 0.34$; Figure S2B).

To assess the significance of different temporal and spatial characteristics of these neuronal assemblies, we generated control null models by shuffling the identity of the neurons composing each assembly. This procedure randomized the topographies of the assemblies while keeping intact the number of neurons per assembly and the topographic position and activity time series of each neuron. Since the level of correlations between pairs of neurons may depend on the frequency of Ca^{2+} events, we chose the null-model assemblies with an average activity similar to that of their respective spontaneous assemblies (within 1 SD). We then normalized the respective values of the temporal and spatial traits of the different assemblies with respect to their corresponding null models.

Consistent with the observation that the majority of the high-correlation coefficients were between neurons belonging to the same tectal hemisphere, the spontaneous neuronal assemblies showed topographies that were often within the boundaries of a single tectal hemisphere (Figure 2C). However, during development, the assemblies presented large differences in terms of topographic dispersion of their neurons. We defined two indexes to assess the evolution of their topography: a *lateralization index* to quantify the distribution of each assembly with respect to both tectal hemispheres (Figure 2D) and a *compactness index* proportional to the topographical density of the neurons within each assembly (Figure 2E). In intact larvae, lateralization and compactness indexes significantly increased upon the arrival of retinal inputs to the tectum at 3 dpf ($p < 10^{-4}$ for both indexes), reaching a plateau at 5 dpf. A slight decrease was observed at 8 dpf ($p < 0.002$ for the lateralization index, and $p = 0.017$ for the compactness index, from 5 to 8 dpf). Noticeably, at 2.5 dpf, the assemblies already tended to be localized within one hemisphere (lateralization index significantly higher than 0; $p < 10^{-3}$). Enucleated larvae showed similar, although delayed, developmental dynamics. At 3 dpf, the average value of lateralization and compactness indexes did not significantly differ from that of 2.5-dpf intact larvae ($p > 0.85$), but they reached values similar to those of intact larvae at 8 dpf ($p > 0.19$ for the lateralization index, and $p > 0.57$ for the compactness index).

Since the spontaneous neuronal assemblies revealed coherent activity of their constitutive neurons, we defined a *matching index* (MI) for each assembly to evaluate their activation dynamics (Figure S2C). The MI was based on the similarity

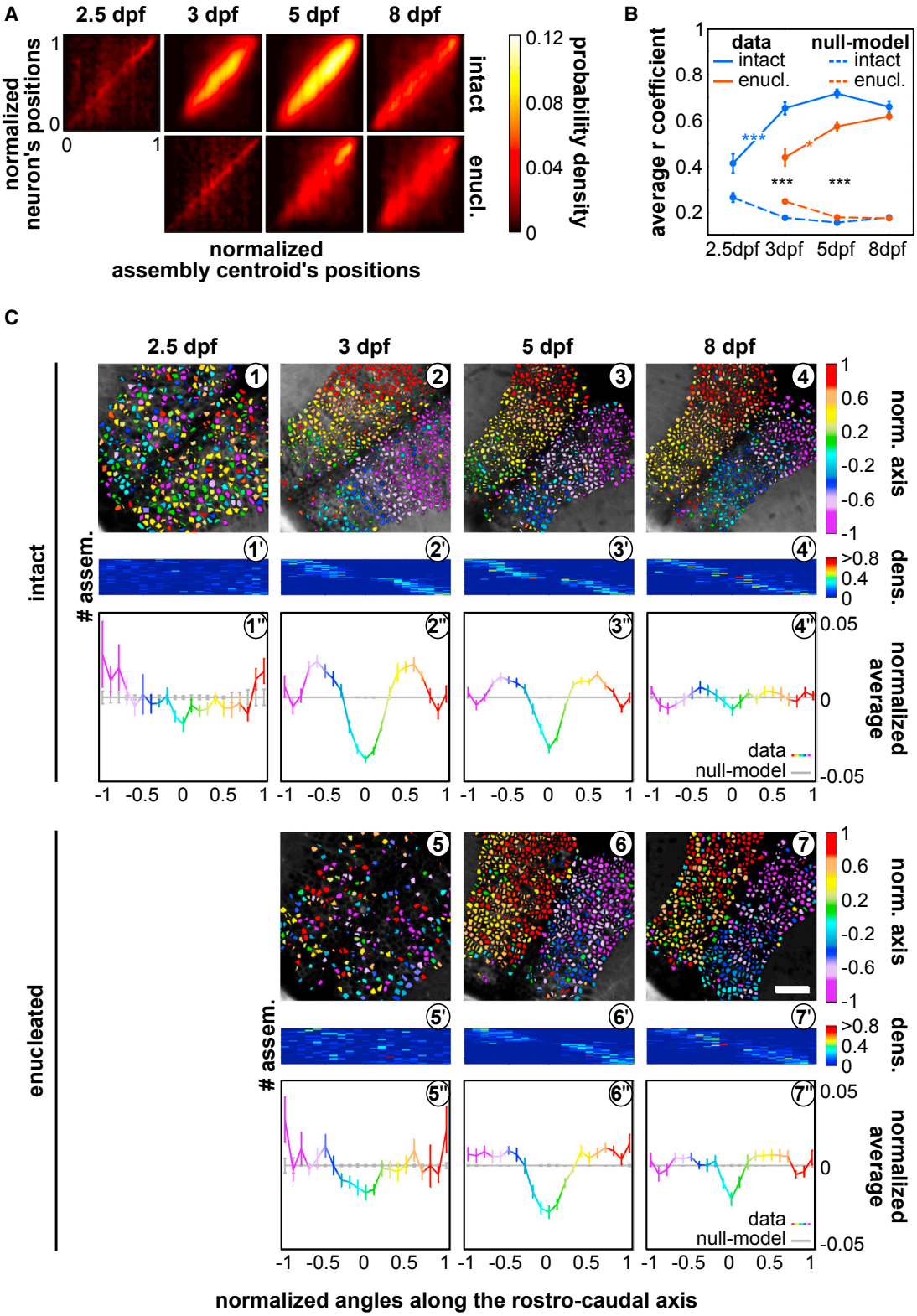

(legend on next page)

between the pattern of active neurons at each imaged frame, with respect to the neurons belonging to a given assembly. It ranges from 0 to 1, where 1 represents a full match between the topography of a given assembly and that of the imaged activity pattern, and 0 represents a complete mismatch. Using this index, we analyzed the temporal dynamics of each neuronal assembly. Each assembly was active several times during the recording period, and their frequency increased significantly throughout development in both intact and enucleated larvae (Figure S2D).

In the functionally mature optic tectum (8 dpf), the spontaneous neuronal assemblies grouped neurons with similar selectivities for spatial positions of the visual field (similar spatial tuning curves) and resembled neuronal response patterns induced by spatially localized visual stimuli (Romano et al., 2015). To establish whether this property is already present at the onset of retinotectal connections, we measured the tectal neuronal responses to light spots of 20°, presented across the visual field of 3-dpf larvae, and compared them to those of 8-dpf larvae (Figures S3A and S3B). We observed that spontaneous assemblies tended to regroup neurons with similar spatial tuning curves (visual receptive fields) in both 3- and 8-dpf larvae (Figures S3C–S3E). These results indicate that the spontaneous neuronal assemblies regroup functionally related neurons already at the onset of retinotectal interactions, further suggesting that the formation of the functional assemblies is, most likely, independent of visual experience.

The tectum is a multisensory structure; its ventral layers receive inputs from the lateral line and the auditory system (Nevin et al., 2010). Therefore, it is possible that the spontaneous assemblies that we observed in the dorsal visual layers of the optic tectum could represent spontaneous activation of other sensory modalities. To control for this possibility, we stimulated the lateral line or the auditory system of zebrafish larvae, while monitoring tectal activity, in intact and enucleated 8-dpf larvae. We observed that these modalities were weakly represented in the ventral part of the tectum of intact larvae, and mostly absent in the dorsal visual layers, in both intact and enucleated larvae (Figures S3F–S3H). These results indicate that the chronic absence of retinal inputs did not generate plastic changes, leading to an increase of the auditory and the lateral line responses in the dorsal visual layers of the optic tectum. We thus suggest that the spatial structure of the ongoing tectal activity, capable of emerging in the absence of retinal inputs, represents the functional connectivity of the tectum associated with its visual role, rather than reflecting other non-visual sensory maps.

Overall, these results suggest that the ongoing spontaneous tectal activity is organized according to functional neuronal assemblies that, during development, become more compact and specific to a single tectal hemisphere. The absence of retinal inputs delayed the maturation of the neuronal assemblies but did not prevent it. In addition, at 8 dpf, intact larvae showed a slight decrease in the compactness and lateralization indices of the assemblies, supporting the idea of the possible emergence of new, extra tectal afferents or intertectal connectivity after 5 dpf.

Spontaneous Neuronal Assemblies Reveal a Tectal Topographic Organization

It was previously shown in the functionally mature network that the spontaneous neuronal assemblies reflect the retinotopic map of the optic tectum (Romano et al., 2015). We asked whether a spatial organization of the tectal spontaneous activity is present even before functional retinotectal interactions, how it changes during maturation, and how it is affected by the chronic deprivation of all retinal inputs. We first determined which tectal morphological axes best described the topographic organization of the neuronal assemblies, according to our imaging plane. We calculated the correlation coefficient (r) of the linear regression between the position of the centroid of each assembly and the position of each of the neurons within the assembly in a common spatial reference (Figure S4A; Niell and Smith, 2005). A strong correlation would indicate that the assemblies are composed of neighboring neurons rather than showing sparse topographies. The axis with the highest r values best fitted the caudo-rostral axis for all developmental stages for both intact and enucleated larvae (Figure S4B). Therefore, we used the average r coefficients along this axis as a measure of the global topographic organization level of tectal spontaneous assemblies and compared them to those of the respective null-models to assess their significance (Figures 3A, 3B, and S4C). Despite the absence of significant temporal correlations, intact larvae showed weak, although significant, topographic organization already at 2.5 dpf ($p < 0.004$ when compared to 2.5-dpf null models), suggesting that a spontaneous activity spatial structure is already present before the retina functionally

Figure 3. The Spontaneous Neuronal Assemblies Progressively Organize along the Tectal Caudo-rostral Axis, during Development

(A) Density plots of the caudo-rostral normalized positions of each neuron against the normalized position of each neuronal assembly centroid along the caudo-rostral axis of the tectum, in intact and enucleated (enucl.) larvae, at each developmental stage; 0 is the most rostral position and 1 is the most caudal one (in the enucleated 8-dpf larva density plot; the respective null models are in Figure S4C).

(B) Average r coefficients of the regression fit between the position of the assembly's centroids and that of the assembly's neurons, along the caudo-rostral axis, in intact (blue) and enucleated (enucl.; red) larvae. The respective null models are depicted by the dashed curves in the right panel. ***$p < 0.001$.

(C) Topographic organization of the spontaneous neuronal assemblies. (1–4) Examples of assemblies' topographies projected along the caudo-rostral axis of an intact larva at different developmental stages. Color bar: position along the caudo-rostral axis (the neurons are color coded according to the centroid azimuthal position of the assembly to which they belong). (5–7) Same as for (1)–(4), but for the enucleated larvae. Scale bar represents 100 μm. (1'–7') Distribution of the density of number of neurons belonging to each assembly, along the normalized (norm.) caudo-rostral axis, for the experiment illustrated in (1)–(7), respectively; y axis: neuronal assembly number (# assem.); x axis: normalized caudo-rostral tectal axis (see Figure S4D for the distributions of all experiments and their respective null models). Color bar: neuronal density along the normalized caudo-rostral axis (dens.). (1''–7'') Average normalized mean distributions of the assemblies' neuronal densities in (1')–(7'), for all experiments during the different developmental stages, in intact and enucleated conditions, color coded accordingly to their normalized azimuthal positions (color bar). The normalized mean distributions of the respective null models are depicted in gray.

Error bars indicate SEM. See also Figure S4.

connects to the tectum and highlighting the early role of molecular cues in the topographic organization of the tectal circuitry. At 3 dpf, this spatial organization significantly strengthened with the arrival of the retinal inputs ($p < 10^{-4}$) and did not significantly change subsequently (3 versus 5 or 8 dpf and 5 versus 8 dpf: $p > 0.14$). In enucleated larvae, the average r coefficient at 3 dpf was not significantly different from that of 2.5-dpf intact larvae ($p > 0.85$), yet it reached values similar to those of intact larvae at 8 dpf ($p > 0.18$).

To estimate how well the different regions of the optic tectum are represented by the spontaneous neuronal assemblies, we calculated the density of neurons within an assembly along the caudo-rostral axis (Figures 3C and S4D). Similar average density values would imply a homogeneous topographic organization where all regions of the larva's field of view are similarly represented by the spontaneous neuronal assemblies. To control for the increasing number of tectal neurons during development, we normalized the density distributions with respect to the null models (Figures 3C1''–3C7'').

Already at 2.5 dpf, the caudal domains of the optic tectum contained assemblies that were topographically denser than in the more frontal regions. This bias was further pronounced at 3 dpf, but it began to recede at 5 dpf and mostly disappeared at 8 dpf (the majority of the regions along the caudo-rostral axis presented a homogeneous distribution of densities, except for the most rostral position; $p = 0.034$; Figures 3C1''–3C4''). Enucleated larvae showed comparable developmental dynamics of average density values, although less pronounced and delayed. The 3-dpf enucleated larvae were similar to the 2.5-dpf intact ones ($p > 0.45$). At 8 dpf, the neuronal density of the assemblies along the caudo-rostral axis was more uniform and matched the topographic representation of intact larvae at the same developmental stage, except for the most rostral position ($p < 0.003$; Figures 3C5''–3C7'').

Overall, these results show that the tectal spontaneous activity has a topographical structure organized along the relevant functional retinotopic axis (Niell and Smith, 2005), which evolves over the course of development to reach a near-uniform distribution of the neuronal assemblies along this axis. The absence of retinal inputs delays, but does not prevent, the development of the spatial structure of the tectal spontaneous activity.

The Spontaneous Neuronal Assemblies Are Functional even in the Chronic Absence of Retinal Inputs

To assess whether the spontaneous assemblies remain functional even in the chronic absence of retinal inputs, we investigated their capacity to predict self-generated motor behaviors (Romano et al., 2015) at a developmental stage at which the optic tectum is functionally mature (8 dpf). Thus, we simultaneously monitored tectal spontaneous neuronal activity and spontaneous tail movements in intact and enucleated larvae (Figures 4A and 4B). In both conditions, larvae produced brief episodes of tail movements of equivalent duration (387 ms ± 32 ms and 388 ms ± 42 ms, respectively, for intact and enucleated larvae), but with a significantly higher frequency in the enucleated larvae (126–158 movements.hr^{-1} versus 59–75 movements.hr^{-1} in intact larvae; 95% confidence interval after a Jack-Knife procedure [$CI_{95\%}$]).

To assess the role of the spontaneous assemblies in predicting self-generated behaviors, we considered only tail movements separated by at least 5 s. In this manner, we ensured that the analyzed tectal activity was directly related to the succeeding movement rather than representing activity associated with the previous one. We observed that topologically compact groups of neurons (compactness index: 0.38 ± 0.04 in intact and 0.31 ± 0.02 in enucleated larvae) were activated just before the onset of the tail movements at a rate of 5.0 episodes.hr^{-1} in intact larvae and 4.8 episodes.hr^{-1} in enucleated larvae. Thus, we computed the chance of observing a self-generated movement, given the spontaneous activation of a tectal compact assembly before the movement. More precisely, we calculated the probability of generating a spontaneous tail movement as a function of the correlation between the patterns of tectal activity preceding the onset of a tail flip and the topographies of all the spontaneous neuronal assemblies found. This correlation indicates the degree of similarity between the activity of the tectal circuit preceding a movement and the topographies of the spontaneous compact neuronal assemblies (Figure 4C). We found that this probability sharply increased as the spontaneous tectal activity gradually matched the topography of the spontaneous assemblies. Surprisingly, the tail movement probability as a function of this correlation was not significantly different in intact and enucleated larvae (mostly overlapping $CI_{95\%}$; Figure 4C). These results indicate that the observed tectal spontaneous assemblies capable of emerging in the chronic absence of visual inputs are still functionally relevant with respect to its motor output.

DISCUSSION

Our results show that, before the formation of functional retinotectal connections, the spontaneous activity of the optic tectum displays characteristics reminiscent of nascent networks, largely composed of neurons in an immature state (Gu et al., 1994; Sheroziya et al., 2009), and weakly interconnected circuits. Right after the onset of retinotectal interactions (at 3 dpf, via excitatory glutamatergic inputs), we measured rapid changes in the network, likely due to the maturation of the different neuronal sub-populations of the tectal network (Sin et al., 2002). This hypothesis is in line with the observed delay in the emergence of the spatiotemporal structure of the spontaneous activity in enucleated larvae. In addition to activity-dependent mechanisms, it is also possible that molecular cues could play a role in the development of the tectum's ongoing spontaneous activity (e.g., secreted factors or cell-adhesion molecules that could be expressed by the RGCs; Triplett, 2014). By 8 dpf, the amplitude, frequency, and synchronization of Ca^{2+} events in enucleated larvae significantly increased above normal values. The early removal of retinal inputs have, therefore, a long-standing effect on the maturation of the tectal neurons reflected by an apparent increase in excitability (Akerman and Cline, 2006; Sernagor et al., 2003).

In addition, we showed that tectal spontaneous activity is significantly correlated at the single-cell level and organized in coherent neuronal assemblies that regroup neurons with similar functional properties and are arranged along the retinotopic tectal axis from the onset of the retinotectal functional

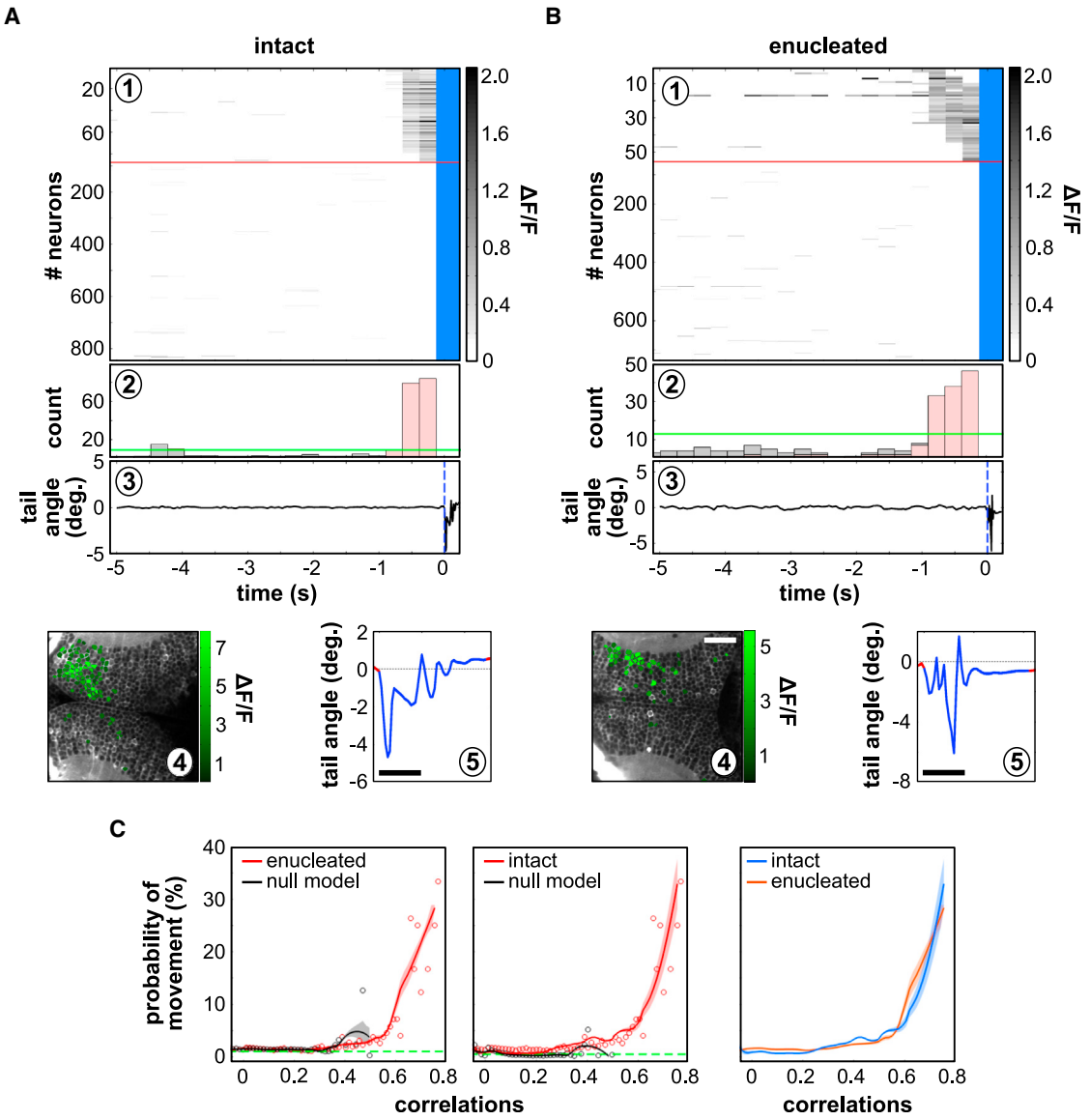

Figure 4. Spontaneous Neuronal Assemblies Are Predictive of Tail Motor Behaviors, even in Chronic Absence of Retinal Inputs

(A and B) Examples of spontaneous activation of a topographically compact tectal assembly before the onset of a tail movement in an intact larva (A) and an enucleated larva (B). (A1 and B1) Raster plot of all imaged tectal neurons; the red line separates the neurons belonging to the active neuronal pattern before the tail flip (above), from the rest of the neurons in the circuit (below; notice that the scale is different above and below the line; blue indicates frames during tail-flip movements). (A2 and B2) Histogram of the number of active neurons in the circuit; the fraction of neurons in the active neuronal pattern is represented in pink; the green line represents the threshold for significant neuronal population events. (A3 and B3) Tail angle. The blue dashed line indicates the onset of tail movement. Deg, degree. (A4 and B4) Topography of the spontaneously active neuronal pattern; compactness index: 0.54 (A4) and 0.33 (B4). (A5 and B5) A magnification of the angle of the tail during the movement. Scale bars, 100 ms.

(C) Probability of a tail movement as a function of the correlation between all assembly patterns and the spontaneous tectal network activity for the imaging frame preceding the movement onset in intact larvae (left; n = 6) and enucleated larvae (middle; n = 6). Red dots indicate raw data; black dots indicate null models; red curves indicate regression fits, with $CI_{95\%}$; black curves indicate null-model assemblies; and dashed green lines indicate global average probability of movements. Right: comparison between intact larvae (blue) and enucleated larvae (red).

connections (see also Romano et al., 2015). In the chronic absence of retinal inputs, the maturation of the spatial structure of the spontaneous activity was delayed with respect to intact larvae. However by 8 dpf, the topographic organization in intact and enucleated larvae became almost indistinguishable, strengthening the idea that neither visual experience nor the retinal patterned spontaneous activity is essential for the establishment of a proper topographic arrangement along the retinotopic axis of the optic tectum. The generation and maintenance of the spatial structure of the spontaneous activity is, thus, likely

determined by an intrinsic mechanism that organizes the circuit architecture of the optic tectum. The fact that the retina promotes the development of the spatial structure of the tectal spontaneous activity at an early stage of the development of the visual system, but is not essential for its further maturation, leads us to hypothesize that the predetermined tectal connectivity is strengthened by the level of retinal drive per se, rather than its patterned sensory inputs.

In the intact mature visual system of zebrafish larvae, the spontaneous activity spatial structure reflects the functional retinotopic tectal map and it is predictive of tail motor movements (see also Romano et al., 2015). We found that the predictive nature of the spontaneous activity in the mature tectum of enucleated larvae was similar to those of intact ones. This implies that, even in the chronic absence of retinal inputs, the tectal network is capable of connecting properly and projecting to its extratectal post-synaptic targets, suggesting that primary sensory inputs to the tectum are dispensable for the development of a functional tectal network.

Conclusions

We have shown that the retina strongly influences the development of the intrinsic connectivity of the optic tectum. However, the absence of visual inputs does not prevent a spatial organization of the spontaneous tectal activity that reveals neuronal assemblies associated with visuomotor transformations, supporting the idea that the tectal network is prone for its functional role. This capability may be an advantageous developmental strategy for the prompt execution of vital behaviors, such as escaping predators or catching prey, without requiring prior visual experience. However, this does not preclude the possibility that visual experience plays a role in the further refinement of the tectal circuitry.

EXPERIMENTAL PROCEDURES

Animals

Zebrafish were maintained on a 14-hr/10-hr light/dark cycle at a temperature of 28.5°C. HuC:GCaMP3^{ens100Tg} zebrafish larvae (Panier et al., 2013) in a Nacre background (mitfa$^{-/-}$) were raised up to 8 dpf, in 0.5× E3 embryo medium (Westerfield, 1995) and fed with paramecia after 5 dpf. All experiments were approved by Le Comité d'Éthique pour l'Expérimentation Animale Charles Darwin (03839.03).

In Vivo Imaging

To monitor the neuronal activity, we used a custom-built two-photon scanning microscope based on a MOM (Movable Objective Microscope) system (Sutter Instruments), with a 25×, NA 1.05 objective (Olympus) and a Mai-Tai DeepSee Ti:sapphire laser (Spectra-Physics) tuned to 920 nm. Collection of the emission light path consisted of FF705 dichroic, FF01-680 short-pass, and FF01 520/70 band-pass filters (Semrock). The photomultiplier tube was an H1070 (GaAsP; Hamamatsu). Its output signal was amplified with an SR-570 low-noise current preamplifier (Stanford Research Systems). The output excitation laser power at the focal plane was less than 3 mW. For data acquisition and controlling the galvanometers, we used ScanImage r3.8 (Pologruto et al., 2003). Data were acquired at ~3.91 Hz, with a resolution of 256 × 256 pixels (~0.262-mm^2 optical plane).

Data Analysis

Image segmentation to obtain regions of interest corresponding to neurons, curation of movement artifacts, and detection of the significant calcium transients were performed as described in Romano et al. (2015), using custom-written MATLAB scripts (MathWorks). Frames with movement artifacts were not further considered, and the non-significant portions of the ΔF/F traces were then set to 0 in all subsequent analysis.

All data were processed using custom-made scripts written in MATLAB. The Kolmogorov-Smirnov test was used for all statistical analyses, unless otherwise noted. In some cases, Wilcoxon signed-rank tests were used when comparisons with zero median were required. For comparisons between groups, we used the Jack-Knife procedure. This procedure is a non-parametric re-sampling method. Each observation is successively left out from a given dataset of n samples before estimating the mean of this sub-dataset. This procedure generates an $n - 1$ number of estimates. The average and variance of all these estimates are then calculated, and the 95% confidence interval is approximated (twice the squared root of the variance divided by n). All measured values were expressed as mean ± SEM. The levels of significance of the comparison between two conditions are: *$p < 0.05$; **$p < 0.01$; and ***$p < 0.001$.

SUPPLEMENTAL INFORMATION

Supplemental Information includes Supplemental Experimental Procedures and four figures and can be found with this article online at http://dx.doi.org/10.1016/j.celrep.2017.04.015.

AUTHOR CONTRIBUTIONS

Conceived and designed the experiments: T.P. and G.S. Performed the experiments: T.P., and J.B.-W. and V.C. for controls. Analyzed the data: T.P. Contributed reagents/materials/analysis tools: T.P., S.A.R., and V.P.-S. Wrote the paper: T.P. and G.S.

ACKNOWLEDGMENTS

The authors thank the members of the lab for their support and discussions, A. Jouary for help with tail movements' analysis, B. Barbour for comments on the manuscript, P. Gongal for editorial assistance, and F. Bouallage for the constant care of zebrafish. This work was supported by ERC stg 243106 (to G.S.), the Fondation pour la Recherche Médicale (to T.P.), ANR-10-LABX-54 (MEMO LIFE), and ANR-11-IDEX-0001-02 (PSL* Research University).

Received: June 14, 2016
Revised: February 15, 2017
Accepted: April 4, 2017
Published: May 2, 2017

REFERENCES

Ackman, J.B., and Crair, M.C. (2014). Role of emergent neural activity in visual map development. Curr. Opin. Neurobiol. *24*, 166–175.

Akerman, C.J., and Cline, H.T. (2006). Depolarizing GABAergic conductances regulate the balance of excitation to inhibition in the developing retinotectal circuit in vivo. J. Neurosci. *26*, 5117–5130.

Burbridge, T.J., Xu, H.-P., Ackman, J.B., Ge, X., Zhang, Y., Ye, M.-J., Zhou, Z.J., Xu, J., Contractor, A., and Crair, M.C. (2014). Visual circuit development requires patterned activity mediated by retinal acetylcholine receptors. Neuron *84*, 1049–1064.

Burrill, J.D., and Easter, S.S., Jr. (1994). Development of the retinofugal projections in the embryonic and larval zebrafish (Brachydanio rerio). J. Comp. Neurol. *346*, 583–600.

Faisal, A.A., Selen, L.P.J., and Wolpert, D.M. (2008). Noise in the nervous system. Nat. Rev. Neurosci. *9*, 292–303.

Fiser, J., Chiu, C., and Weliky, M. (2004). Small modulation of ongoing cortical dynamics by sensory input during natural vision. Nature *431*, 573–578.

Gahtan, E., Tanger, P., and Baier, H. (2005). Visual prey capture in larval zebrafish is controlled by identified reticulospinal neurons downstream of the tectum. J. Neurosci. *25*, 9294–9303.

Gu, X., Olson, E.C., and Spitzer, N.C. (1994). Spontaneous neuronal calcium spikes and waves during early differentiation. J. Neurosci. *14*, 6325–6335.

Huberman, A.D., Feller, M.B., and Chapman, B. (2008). Mechanisms underlying development of visual maps and receptive fields. Annu. Rev. Neurosci. *31*, 479–509.

Jetti, S.K., Vendrell-Llopis, N., and Yaksi, E. (2014). Spontaneous activity governs olfactory representations in spatially organized habenular microcircuits. Curr. Biol. *24*, 434–439.

Keck, T., Keller, G.B., Jacobsen, R.I., Eysel, U.T., Bonhoeffer, T., and Hübener, M. (2013). Synaptic scaling and homeostatic plasticity in the mouse visual cortex in vivo. Neuron *80*, 327–334.

Kenet, T., Bibitchkov, D., Tsodyks, M., Grinvald, A., and Arieli, A. (2003). Spontaneously emerging cortical representations of visual attributes. Nature *425*, 954–956.

Kirkby, L.A., Sack, G.S., Firl, A., and Feller, M.B. (2013). A role for correlated spontaneous activity in the assembly of neural circuits. Neuron *80*, 1129–1144.

Kita, E.M., Scott, E.K., and Goodhill, G.J. (2015). Topographic wiring of the retinotectal connection in zebrafish. Dev. Neurobiol. *75*, 542–556.

Krauzlis, R.J., Lovejoy, L.P., and Zénon, A. (2013). Superior colliculus and visual spatial attention. Annu. Rev. Neurosci. *36*, 165–182.

Nevin, L.M., Robles, E., Baier, H., and Scott, E.K. (2010). Focusing on optic tectum circuitry through the lens of genetics. BMC Biol. *8*, 126.

Niell, C.M., and Smith, S.J. (2005). Functional imaging reveals rapid development of visual response properties in the zebrafish tectum. Neuron *45*, 941–951.

Panier, T., Romano, S.A., Olive, R., Pietri, T., Sumbre, G., Candelier, R., and Debrégeas, G. (2013). Fast functional imaging of multiple brain regions in intact zebrafish larvae using selective plane illumination microscopy. Front. Neural Circuits *7*, 65.

Pologruto, T.A., Sabatini, B.L., and Svoboda, K. (2003). ScanImage: flexible software for operating laser scanning microscopes. Biomed. Eng. Online *2*, 13.

Pratt, K.G., Dong, W., and Aizenman, C.D. (2008). Development and spike timing-dependent plasticity of recurrent excitation in the Xenopus optic tectum. Nat. Neurosci. *11*, 467–475.

Romano, S.A.A., Pietri, T., Pérez-Schuster, V., Jouary, A., Haudrechy, M., and Sumbre, G. (2015). Spontaneous neuronal network dynamics reveal circuit's functional adaptations for behavior. Neuron *85*, 1070–1085.

Sernagor, E., Young, C., and Eglen, S.J. (2003). Developmental modulation of retinal wave dynamics: shedding light on the GABA saga. J. Neurosci. *23*, 7621–7629.

Sheroziya, M.G., von Bohlen Und Halbach, O., Unsicker, K., and Egorov, A.V. (2009). Spontaneous bursting activity in the developing entorhinal cortex. J. Neurosci. *29*, 12131–12144.

Sin, W.C., Haas, K., Ruthazer, E.S., and Cline, H.T. (2002). Dendrite growth increased by visual activity requires NMDA receptor and Rho GTPases. Nature *419*, 475–480.

Smith, M.A., and Kohn, A. (2008). Spatial and temporal scales of neuronal correlation in primary visual cortex. J. Neurosci. *28*, 12591–12603.

Stuermer, C.A. (1988). Retinotopic organization of the developing retinotectal projection in the zebrafish embryo. J. Neurosci. *8*, 4513–4530.

Sumbre, G., Muto, A., Baier, H., and Poo, M.M. (2008). Entrained rhythmic activities of neuronal ensembles as perceptual memory of time interval. Nature *456*, 102–106.

Tian, L., Hires, S.A., Mao, T., Huber, D., Chiappe, M.E., Chalasani, S.H., Petreanu, L., Akerboom, J., McKinney, S.A., Schreiter, E.R., et al. (2009). Imaging neural activity in worms, flies and mice with improved GCaMP calcium indicators. Nat. Methods *6*, 875–881.

Tolhurst, D.J., Movshon, J.A., and Dean, A.F. (1983). The statistical reliability of signals in single neurons in cat and monkey visual cortex. Vision Res. *23*, 775–785.

Triplett, J.W. (2014). Molecular guidance of retinotopic map development in the midbrain. Curr. Opin. Neurobiol. *24*, 7–12.

Vislay-Meltzer, R.L., Kampff, A.R., and Engert, F. (2006). Spatiotemporal specificity of neuronal activity directs the modification of receptive fields in the developing retinotectal system. Neuron *50*, 101–114.

Warp, E., Agarwal, G., Wyart, C., Friedmann, D., Oldfield, C.S., Conner, A., Del Bene, F., Arrenberg, A.B., Baier, H., and Isacoff, E.Y. (2012). Emergence of patterned activity in the developing zebrafish spinal cord. Curr. Biol. *22*, 93–102.

Weliky, M., and Katz, L.C. (1999). Correlational structure of spontaneous neuronal activity in the developing lateral geniculate nucleus in vivo. Science *285*, 599–604.

Westerfield, M. (1995). The Zebrafish Book: A Guide for the Laboratory Use of Zebrafish (Danio rerio) (University of Oregon Press).

Xu, H., Khakhalin, A.S., Nurmikko, A.V., and Aizenman, C.D. (2011). Visual experience-dependent maturation of correlated neuronal activity patterns in a developing visual system. J. Neurosci. *31*, 8025–8036.

Zhou, Q., Tao, H.W., and Poo, M.M. (2003). Reversal and stabilization of synaptic modifications in a developing visual system. Science *300*, 1953–1957.

Cell Reports, Volume *19*

Supplemental Information

The Emergence of the Spatial Structure of Tectal Spontaneous Activity Is Independent of Visual Inputs

Thomas Pietri, Sebastián A. Romano, Verónica Pérez-Schuster, Jonathan Boulanger-Weill, Virginie Candat, and Germán Sumbre

Supplemental figures

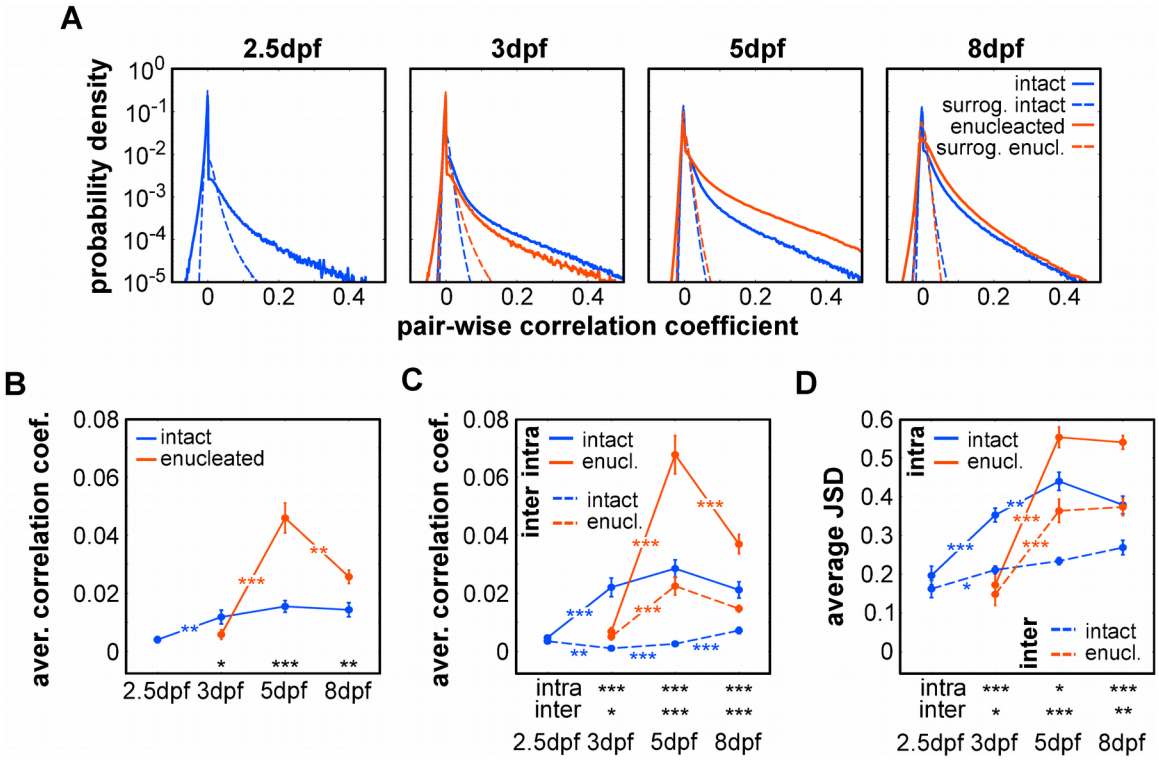

Figure S1: Pair-wise correlations between tectal neurons for all developmental stages in intact and enucleated larvae, related to Figure 1.
(**A**) Probability density of the distributions of the Pearson's correlation coefficients between neuronal pairs, per developmental stage, in intact and enucleated larvae. The dashed curves depict the respective random surrogate versions. The distributions were calculated using correlation value bins of 0.001 ranging from -1 to 1. (**B**) Developmental dynamics of the average correlation coefficients for all neurons, in intact and enucleated larvae. (**C**) Average correlation coefficients for all pairs of neurons belonging to the same tectal hemisphere ('intra', solid curve) and all pairs of neurons belonging to different tectal hemispheres ('inter', dashed curve), in intact and enucleated larvae. (**D**) Average JSD for each stage in enucleated and intact conditions, for the pair-wise correlations of neurons belonging to the same tectal hemisphere ('intra', solid curve) and to both hemispheres ('inter', dashed curve). Comparison between stages are indicated on the curves (blue and red) and between intact and enucleated groups, at the bottom of the graph in black. Blue and red: intact and enucleated larvae respectively; $p < 0.001$: ***; $p < 0.01$: **; $p < 0.05$: *; Error bars: SEM.

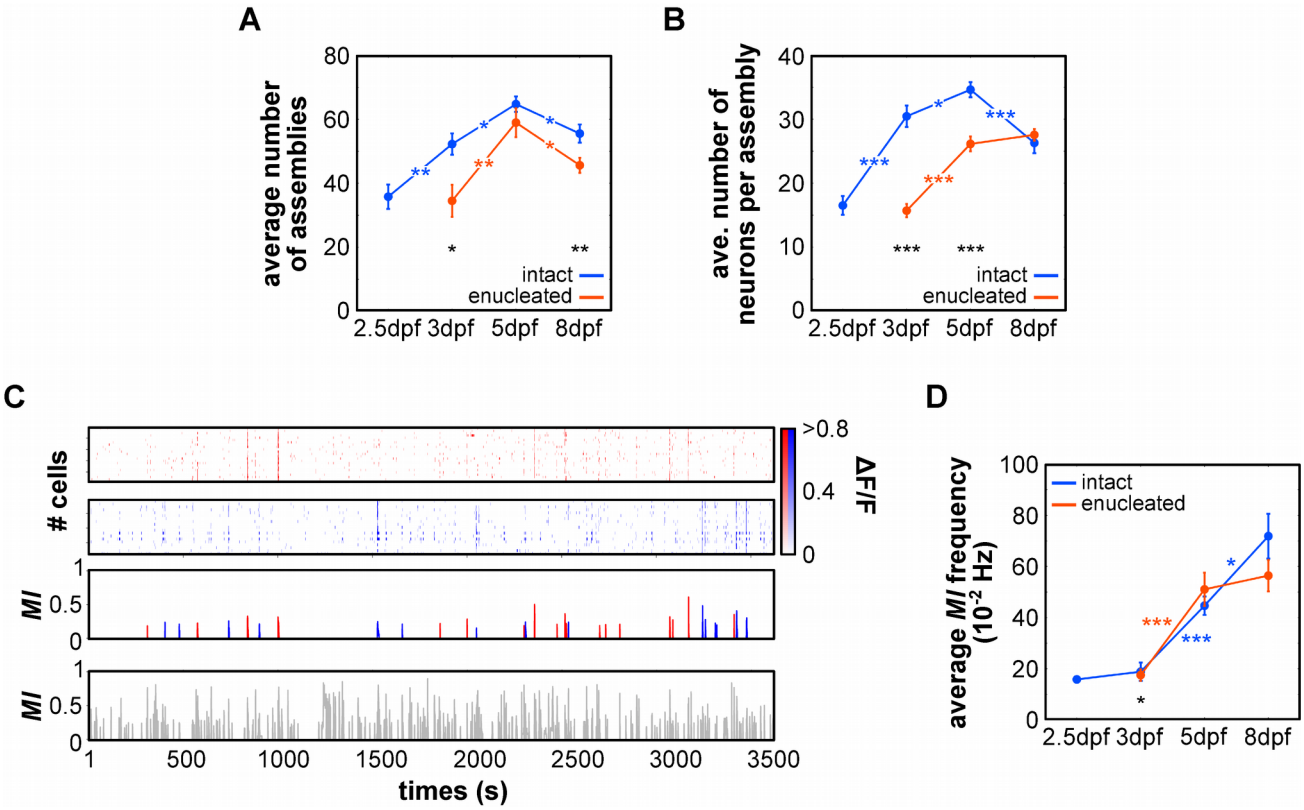

Figure S2: Characterization of the neuronal assemblies, related to Figure 2.
(**A**) Average number of assemblies during development in intact and enucleated larvae. Although the average number of neuronal assemblies in the enucleated larvae are statistically smaller than the aged-match intact larvae (but at 5 dpf: $p = 0.27$), the trend over development is similar when comparing intact and enucleated larvae, with an increase in the number of extracted assemblies up to 5 dpf, followed by a decrease at 8 dpf. This trend is in line with the variation of the level of correlations observed for the whole neuronal population. (**B**) Average number of neurons per assembly during development in intact and enucleated larvae. In intact larvae, the average number of neurons per assembly increased up to 5 dpf, before sharply falling at 8 dpf (5 vs 8 dpf, $p < 5.10^{-4}$). In enucleated larvae, the average number of neurons per assembly show similar, although delayed, developmental dynamics and by 8 dpf this number is similar in intact and enucleated larvae ($p = 0.18$). (**C**) Raster plots of the significant Ca^{2+} events of the neurons composing two representative neuronal assemblies of a 5 dpf intact larva (top panels), their *matching index* (*MI*, in red and blue respectively, middle panel) and the *matching indexes* of the full population of assemblies (n = 64) of the same 5 dpf larva (bottom panel); peaks level with p values < 0.01 (i.e > 99% confidence) are considered significant. Scale bar: ΔF/F. (**D**) Average *MI* frequency during development in intact and enucleated larvae. No statistical difference are noticeable between intact and enucleated larvae, but at 3 dpf ($p = 0.03$). At this age the average frequency of *MI*s in enucleated larvae is however not different from the one of the intact 2.5 dpf larvae ($p = 0.08$). Blue and red in A, B and D: intact and enucleated larvae respectively; $p < 0.001$: ***; $p < 0.01$: **; $p < 0.05$: *; Error bars: SEM.

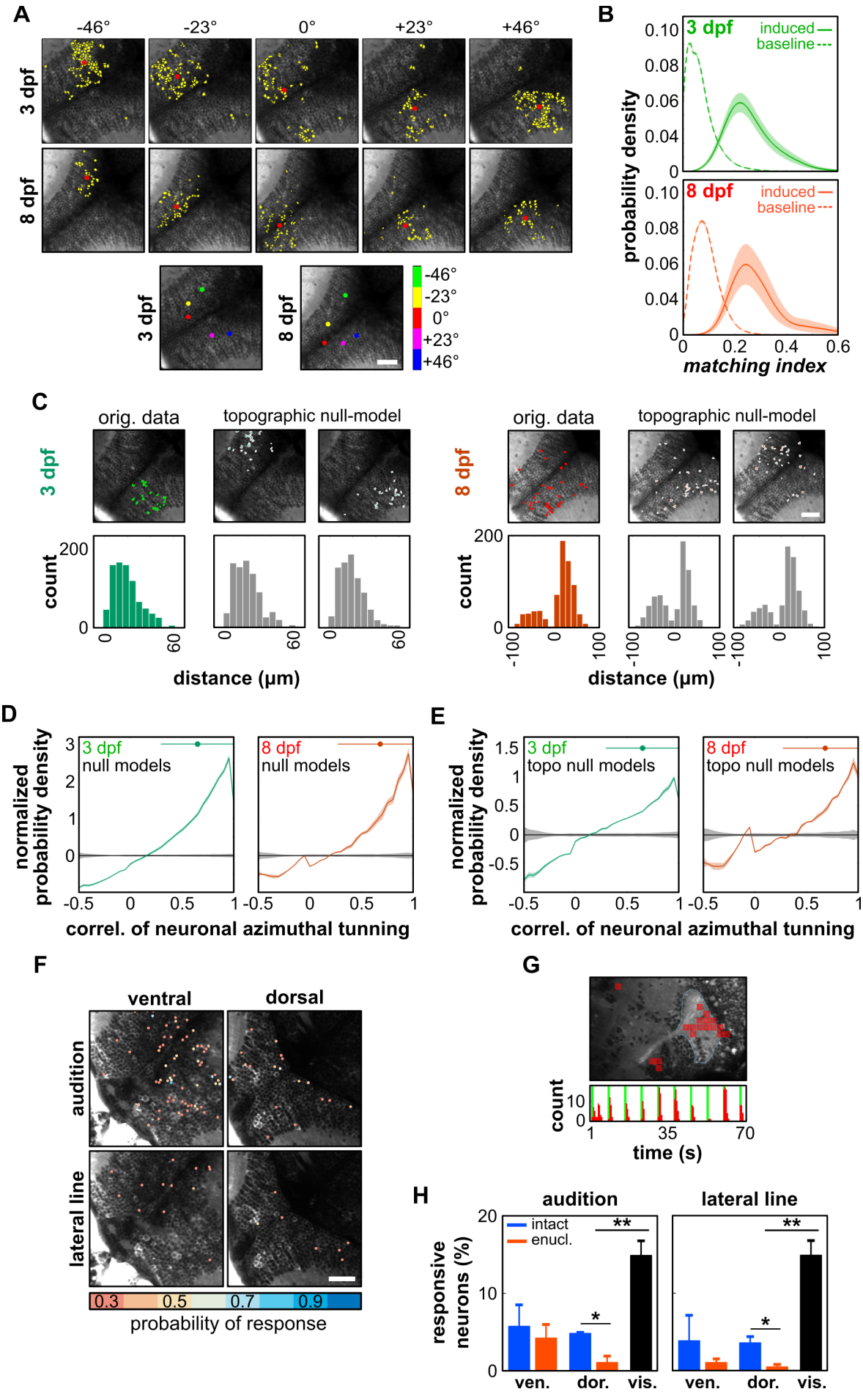
A
-46°
-23°
0°
+23°
+46°
3 dpf
8 dpf
-46°
-23°
0°
+23°
+46°
B
3 dpf
induced
baseline
8 dpf
induced
baseline
probability density
matching index
C
orig. data
topographic null-model
3 dpf
8 dpf
count
distance (μm)
D
3 dpf
null models
8 dpf
null models
normalized probability density
correl. of neuronal azimuthal tunning
E
3 dpf
topo null models
8 dpf
topo null models
normalized probability density
correl. of neuronal azimuthal tunning
F
ventral
dorsal
audition
lateral line
probability of response
G
count
time (s)
H
audition
lateral line
intact
enucl.
responsive neurons (%)
ven.
dor.
vis.

Figure S3: Spontaneous neuronal assemblies regroup functionally related neurons, related to Figure 2.
(**A**) Examples of neuronal assemblies induced by light-spots of 20° angular size, across the visual field (from -46° to +46°) at 3 and 8 dpf; the center of mass of each visually induced assembly is indicated by a red dot; these dots are color-coded in the bottom panels according to the position of the visual stimulus that induced the response. Note the match between the order of the colors along the caudo-rostral axis and the colors representing the different positions of stimulation, indicating that the tectal retinotopic map is organized along the tectal caudo-rostral axis. (**B**) Probability density distributions of the *MI*s of the significant visually induced neuronal groups (3 dpf: green; 8 dpf: red), during the periods of spontaneous activity. The dashed curves represent the distribution of the non-significant *MI* values (baselines). Note that distributions and magnitudes of induced assemblies were comparable at 3 and 8 dpf: the probability density peaks of the significant matching index were 0.226 ± 0.013 at 3 dpf and 0.254 ± 0.013 at 8 dpf, while the ones of their respective baseline were 0.047 ± 0.006 ($p < 10^{-5}$ by comparing *MI*s and baselines) and 0.067 ± 0.004 ($p < 10^{-4}$). (**C**) Examples of 3 dpf (left panels) and 8 dpf (right panels) spontaneous assemblies and corresponding two topographic null assemblies (out of 50). Notice that the distributions of the distance between pair of neurons in the assembly and their respective null model assemblies are similar (bottom panels); positive and negative distance correspond to intra- and inter-hemisphere neuronal pairs, respectively. (**D**) Distribution of the normalized probability density of the pooled pair-wise correlation coefficients of the spatial tuning curves (azimuth tuning curves) of neurons belonging to spontaneous assemblies at 3 (green) and 8 dpf (red) and their respective null models (black). For the normalization, the distributions were divided by the null-model distributions. Note the large bias of the spontaneous assemblies toward grouping neurons with highly similar tuning curves, both at 3 and 8 dpf. The confidence intervals were calculated with a Jack-Knife procedure, across experiments. The significant bias range and median are indicated by the top line and the dot, respectively. The bias ranges became significant above 0.32 ± 0.01 and 0.26 ± 0.08, with medians of 0.633 ± 0.004 and 0.642 ± 0.003, for 3 and 8 dpf larvae respectively (the medians between stages were not statistically different: $p = 0.116$). (**E**). Same as D, but the normalization was performed using the distribution of the topographic null-models. Remarkably, the original assemblies still had a significant bias toward neurons with similar tunings, despite the preservation of the distribution of pair-wise distances in these topographic null-models. (**F**) Examples of topographic localization of the neurons responding to at least 25% of the auditory (top panels) or lateral line stimuli (bottom panels) in a ventral (left panels) and a dorsal (right panels) layer of the optic tectum. The scale bar indicates the probability of response (resp.) of the neurons to at least 25% of the stimuli. (**G**) To test whether the weak tectal response to lateral line stimuli is a direct consequence of lateral line stimulation failure, we monitored the response in the *torus semicircularis* (*TS*, its neuropil is outlined by a pale dashed blue line). Regions of interest (ROIs, delineated out of a homogeneous 10 x 10 pixels grid) in red show the *TS* regions responding to at least 25 % of the stimuli. The histogram of the significant Ca^{2+} events of the ROIs show a reliable and strong response to lateral line stimuli in the *TS*. (**H**) Proportion of neurons responding to at least 25 % of the auditory (left panel) and lateral line (right panel) stimuli, in intact (n = 3, blue) and enucleated larvae (n = 3, red). The proportion of responsive neurons to visual stimulation (vis., moving bar across the visual field) in the dorsal layer of the optic tectum (n = 13, black). Note the significant large differences of the visual responses with respect to the auditory and lateral line ones ($p < 0.005$). In the ventral layers (vent.) of the optic tectum, we observed no significant differences between intact and enucleated larvae for auditory and lateral line responses ($p > 0.97$). In the dorsal layers (dor.), the proportion of cells responding to the stimulation tends however to be smaller in the enucleated than in the intact larvae ($p < 0.04$). Error bars: SEM.

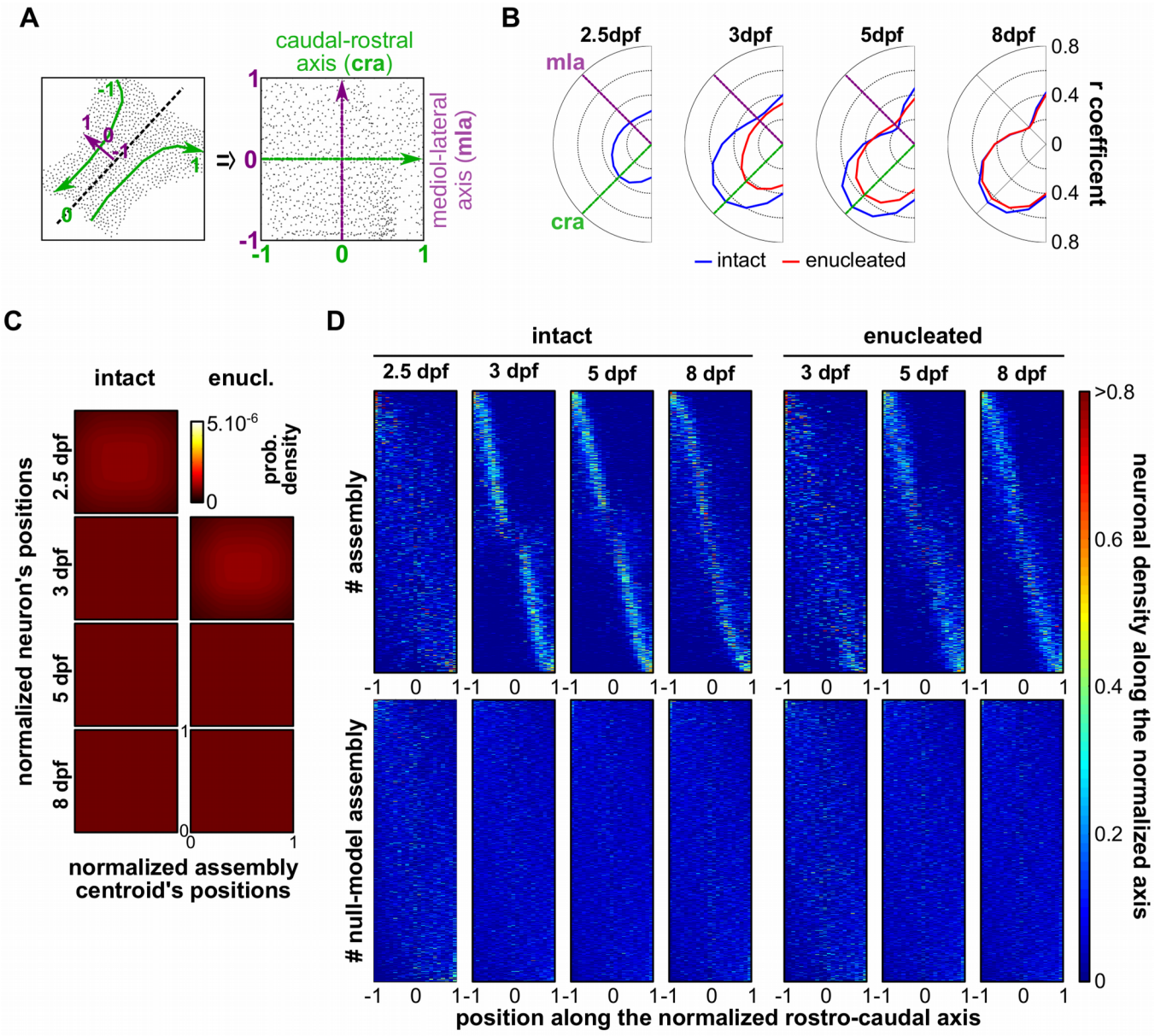

Figure S4: The neuronal assemblies are distributed along the caudo-rostral axis, related to Figure 3.
(**A**) Example of normalization of the neuronal coordinates in a common spatial reference map, where each dot represents a neuron in its original position (left) and after the normalization (right); the morphological medio-lateral (mla) and caudo-rostral axis (cra) are represented in green and purple, respectively. (**B**) Correlation coefficients between the neurons belonging to each assembly and their respective centroids along different axes of the common spatial reference map, rotated every 15° for a total of 180°, for each tectum and for all developmental stages, in intact (blue) and enucleated (red) larvae. Note that the highest correlations were obtained along the tectal caudo-rostral axis in all considered conditions. (**C**) Null-model density plots of the caudo-rostal normalized positions of each neuron against the normalized position of each neuronal assembly centroid, along the caudo-rostral axis of the tectum, in intact and enucleated larvae, at each developmental stage; 0 is the most rostral position and 1, the most caudal one (indicated in the enucleated 8 dpf larva density plot). (**D**) Distribution of the density of the neurons per assembly along the normalized caudo-rostral axis (the axis was normalized between -1 to 1, from lateral left to lateral right) at all developmental stages, in intact (n = 622, 800, 1101 and 864 assemblies for 2.5, 3, 5 and 8 dpf stage respectively) and enucleated larvae (n = 511, 768 and 688 assemblies for 3, 5 and 8 dpf stage, respectively) and their respective null models (built from 50 repetitions of each neuronal assembly). Each neuronal assemblies are represented on the y-axis.

Supplemental Experimental Procedures

Surgical procedures

Since the connection between retina and optic tectum becomes functional at ~ 73 hpf (first visually induced responses in the optic tectum, Niell et al., 2005), we chose to perform bi-lateral ablations of the eyes on 54 - 58 hpf embryos. Enucleations at this stage led the tectal circuit to develop under normal conditions, just before the onset of the functional retinal inputs, therefore, leaving the tectum in a naive state with respect to the visual inputs (retinal spontaneous activity and visual induced activity). Embryos were placed in 1.8 % low-melting agarose with 0.02% MS-222 (anesthetic; Sigma-Aldrich, France) in high-Ca^{2+} Ringer solution (116 mM NaCl, 2.9 mM KCl, 10 mM $CaCl_2$, 5 mM HEPES, pH 7.2) for immobilization purposes, and then submerged in a high-Ca^{2+} Ringer solution. Custom-made micro-scalpel (fabricated from insect pins) were used the remove the eyes of the embryos. In order to assure the complete ablation of the retina and prevent any regeneration, we paid particular attention on the full removal of the photoreceptor layer. The enucleation procedure took just a few minutes and the embryos recovered from anesthesia a few seconds later after being released from the agarose. The embryos were then allowed to recover from the surgery in high-Ca^{2+} Ringer solution, at 28.5°C for two hours, before to be returned to 0.5x E3 embryo medium. In an attempt to feed enucleated larvae after 5 dpf, we added to their Petri dish large amounts of paramecia. This procedure showed limited success, precluding the use of enucleated larvae beyond 8 dpf.

In addition to the enucleations at 54-58 hpf, we performed enucleations at 48 hpf (the time at which the very first RGC axons reach the optic tectum, although these axons have not yet generated functional synapses; n = 3). To control for the effects of the surgical procedure, we also performed sham experiments (n = 3) in which the spinal cord were incised at 55-57 hpf at the level of the cloaca. These two sets of experiments were then compared with the 54-58 hpf enucleated and intact larvae, respectively. For the comparison, we measured two key parameters assessing the temporal and spatial components of the spontaneous activity, namely the Jenson-Shannon distance (JSD, Figure 1F), and the r coefficient of the linear regression of the normalized neuron's positions against the neuronal assembly centroid's positions along the caudo-rostal axis (Figure 3B), at 8 dpf for the 48 hpf enucleations and 5 dpf for the sham experiments. No statistical differences could be observed between the larvae enucleated at 54-58 hpf and those enucleated at 48 hpf (JSD = 0.46 ± 0.02 vs. 0.52 ± 0.04; $p > 0.34$ (Kolmogorov-Smirnov test), and r = 0.615 ± 0.012 vs. 0.618 ± 0.013; $p = 0.70$). Also, no statistical difference could be observed between the sham control experiments and the intact larvae (JSD = 0.27 ± 0.04 SEM vs. 0.29 ± 0.02 SEM, $p > 0.91$ and r = 0.70 ± 0.04 SEM vs. 0.71 ± 0.02 SEM, $p > 0.98$). These control experiments suggest that the enucleations performed at 54-58 hpf efficiently precluded retinal activity influence on the early tectal circuit maturation, without adversary impacting the global development of the larvae due to the surgical procedure.

Choice of the tectal regions for imaging

Larvae were embedded in 2 % low-melting agarose in 0.5x E3 embryo medium, ventral side down on an elevated stage placed in a cylindrical chamber filled with 0.5x E3 embryo medium, and let to adapt for at least 20 min, at room temperature (~ 22 °C) in the dark, before the onset of the experiments.

We imaged the optical section that best responded to visual stimuli. For this purpose, we presented light bars moving across the visual field, while focusing at different depths (z-planes) of the optic tectum. Stimuli were projected on a screen (#216 White Diffusion, Rosco Cinegel) placed around the circular imaging chamber via a pico-projector (Pocket Projector ADPP-305, Adapt). To avoid interference of the visual stimulus with the GCaMP3 emitted fluorescence (peaking at 547 nm and filtered using a 520/50 band-pass filter), only the red LED of the projector was used (620 nm). In addition, a 561 nm long-pass filter (BLP01-561, Semrock, USA) was placed in the front of the projector. Visual stimuli were created using the Psychtoolbox (Brainard, 1997) for Matlab (The MathWorks, Inc.) and designed to compensate for the curvature of the chamber.

The z-planes that best responded to the visual stimuli were observed in the superficial layers of the optic tectum, at depths of ~ 40 – 50 mm (with respect to the dorsal skin) for the 3 dpf larvae, and ~ 60 – 70 mm for the 5 and 8 dpf larvae. For the 2.5 dpf larvae, not responding to visual stimuli, we used the same depth as for the 3 dpf larvae. We used the same imaging depths for the enucleated larvae experiments and several anatomical landmarks, especially the distinctive morphology of the cerebellar region, immediately caudal to the tectum (for instance the lateral positioning of the parallel fibers crossing our optical plan of interest) and the anatomy of the rostral part of to the tectum (characteristic triangular shape), to assure similar positioning of optical planes between larvae at each developmental stage. This strategy enabled us to find similar optical planes of the optic tectum across the different intact and enucleated larvae, at each developmental stage.

To control for unwanted sensory stimulation, the larvae were placed in a complete dark environment, the medium in the large recording chamber was static (no medium flow), and the microscope was place on a 500 kg active air table to filter out vibrations from and outside the table. We also paid a particular attention to perform all experiments in an isolated room away from external noise sources. We thus considered that under these sensory-suppressed conditions, the zebrafish larvae did not experience any sensory stimulation.

Visual stimulation

To accurately assess the onset of the functional connection between the retina and the optic tectum, we continuously imaged

larvae from 70 to 74 hpf at different depths of the optic tectum, while presenting moving light bars. We confirmed that the first response to visual stimuli was observed at ~ 73 hpf (as in Niell and Smitth, 2005) with a variability of less than one hour. Accordingly, experiments were stopped before reaching 72 hpf for the 2.5 dpf stage, and started after 74 hpf for the 3 dpf stage.

For some experiments, we estimated the receptive field of the neurons (spatial tuning curves) by presenting the zebrafish larvae with light spots of 20° in size at different azimuthal angles of the visual field (between -46° to 46°). Light-spot stimuli were presented four times at each position in a random order. We then averaged the neuronal responses induced by stimuli at the same spatial position. Induced responses were calculated over a 2-s window after the onset of the stimulus. Neurons were considered responsive to visual stimuli if they had a significant Ca^{2+} event of an average amplitude response larger than one standard deviation of the average amplitude, and responded to at least 50 % of the stimuli. This procedure enabled us to group neurons in visually induced neuronal groups.

For some experiments, we simultaneously monitored the calcium dynamics in the tectum and the tail movements of the larva. For that purpose, we removed agarose around the tail and added a custom-made small microscope from the ventral side of the larva. This small microscope was connected to a high-speed camera (TXG02, Baumer), controlled by a custom-made script written in C++. Visual stimuli and tail images (acquired at 200 Hz) were both synchronized with the two-photon calcium imaging acquisition software, via a TTL pulse generated by an I/O board (ActiveWire or Arduino) and controlled by Matlab.

Auditory and lateral line stimulation

Auditory stimuli were delivered via a water-proof Visaton K28 miniature speaker placed in front of the larvae within a circular recording chamber. The chamber dimensions were 100 mm of diameter and 50 mm tall, and it was filled with 0.5X E3 medium. The larvae were placed on an elevated stage in the center of the chamber facing the speaker. Stimuli consisted of sinusoids of 1 s duration gated with a 150 ms cosine squared window to prevent spectral leakage. Recordings of the stimulation with a hydrophone (Bruel & Kjaer 8103) showed spectrograms with single pure tones without harmonics. For stimulation of the auditory system we used 600 Hz and for the lateral line, 30 Hz. We presented to each larva 10 stimuli repetitions with an inter-trial time interval of 6 s. Using two-photon Ca^{2+} imaging, we monitored the responses at two different layers of the tectum, namely the visual layer (superficial) where all other experiments were performed, and in a ventral tectal layer, known to receive multisensory information, approximately at the level of the intertectal commissure. Neurons were considered responsive to auditory or lateral line stimuli if they had a significant Ca^{2+} event of an average amplitude response larger than one standard deviation of the average amplitude, and responded to at least 25 % of the stimuli. This procedure enabled us to group neurons in auditory and somatosensory induced neuronal groups.

Data analysis: Ca^{2+} dynamics data processing and detection of neuronal assemblies

Image segmentation to obtain regions of interest corresponding to neurons, curation of movement artifacts and detection of the significant calcium transients were performed as described in Romano et al. (2015), using custom-written Matlab scripts (The MathWorks, Inc.). Frames with movement artifacts were not further considered and the non-significant portions of the ΔF/F traces were then set to 0 in all subsequent analysis. To extract the functional neuronal assemblies from the GCaMP3 fluorescence fluctuations recorded in zebrafish larvae, we use the analytical framework established by Romano et al. (2015).

Briefly, regions of interest corresponding to single neurons were semi-automatically detected using a watershed-based algorithm from an average across the entire time series images. Movement artifacts were automatically detected and discarded. We developed a method to infer the statistical significance of single-neuron calcium transients using a data-driven noise model and imposed biophysical constraints of the fluorescent calcium indicator. All further analysis was performed on significant calcium events. To extract functional neuronal assemblies, we started by representing the spontaneous activity of the entire neuronal population in a space of reduced dimensionality through principal component analysis (PCA), by only keeping principal components (PCs) with significant eigenvalues (Peyrache et al., 2010). To further partition the data into groups of co-varying neurons, we used factor analysis (*promax*) which broke the PCA orthogonality condition (Lopes-dos-Santos et al., 2013). Following this analysis, the PC loadings tended to sparsely concentrate along the non-orthogonal rotated PCs. We then defined the neuronal composition of the assemblies by setting a data-driven threshold on the PC loadings along these non-perpendicular rotated PCs.

Matching index

To analyze the temporal dynamics of the activation of the neuronal assemblies, we implemented a *Dice coefficient* index (*Dc*) previously used to evaluate the degree of similarity in the connection patterns of brain regions (Hilgetag et al., 2002; Sporns et al., 2007). This index first measures the proportion of active neurons at each time point of the recording period (each frame) in both the spontaneous neuronal assembly and the full neuronal population, creating two neuronal activation patterns. Then it quantifies the proportion of neuronal activation that is common to both patterns, with respect to the total number of neuronal activation in each pattern. The neuronal assembly *matching index* ranges between 1, where there is no overlap between the respective patterns and 0 where there is a complete overlap between the respective patterns, at each time frame. We used the hypergeometric distribution to evaluate the probability of observing a common activation pattern by chance (at $p < 0.01$), which estimate the significance of the assembly activation patterns. For this analysis we considered that the neuronal activations were independent

from each other.

Random surrogates and Jensen-Shannon distances
To assess the statistical significance of the pair-wise correlations of neuronal activities across different developmental stages, we generated random surrogate data sets. This is particularly important when comparing experiments, with different neuronal activity dynamics (e.i. frequency of significant neuronal Ca^{2+} events). To this end, we repeatedly shuffled the time stamp of significant Ca^{2+} events of each neuron and observed that 50 repetitions of this procedure were sufficient to create a surrogate data set, as adding more repetitions did not change neither the mean nor the variance of different measured parameters of the surrogate data set.

To test whether the pair-wise Pearson's correlation coefficients can be indicative of a structure in the spontaneous activity (in contrast to correlations explained by chance), we measured the Jensen-Shannon distance (JSD) between the distribution of the spontaneous correlation coefficients and distribution of the respective random surrogate sets. The JSD is a metric measurement of the dissimilarity between two distributions. It is derived from the classical information-theory Kullback-Leibler divergence (Kld), with the advantage of being a dimensionless and symmetric measure (Lin, 1991).

$$KLd(p1 \| p2) = \sum_r p1(r) \log \frac{p1(r)}{p2(r)}$$

and

$$JSD(p1 \| p2) = \sqrt{\frac{KLd(p1 \| q) + KLd(p2 \| q)}{2}} \quad \text{, where} \quad q = \frac{p1 + p2}{2}$$

p1 is the probability distribution of the correlation coefficients of the data, and *p2*, of the random surrogates, at each discrete bin r along the distributions. We used a base 2 logarithm to calculate the *Kld* to bound the JDS between 0 and 1.

Null models of the neuronal assemblies for the significance assessment of the different features
To assess the significance of the topographic and dynamic features of the neuronal assemblies, we compared them against surrogate assembly null models. We shuffled the indexing (neuronal identity) of the entire neuronal population for each experiment and then built null models by grouping neurons according to the original assemblies, but using the shuffled neuronal indexes. We created 50 sets of randomly shuffled surrogate assemblies. This procedure randomized the topography of each assembly, while keeping intact the number of neurons per assembly and, the topographical position and activation time series of each neuron. Since pair-wise correlations can be sensitive to the amount of neuronal activity, we selected the null-model assemblies according to their average level of activity. We kept those within mean ± standard deviation of the activity level of the considered assembly. In some cases, we also built random shuffle assembly null model, with the constraint of conserving the distribution of relative pair-wise physical distances between neurons found in the original assemblies. For a given spontaneous assembly, we randomly chose a first neuron in the contralateral tectum and iteratively added neurons to the topographic null model in a way that conserved the neuron pair-wise assembly physical distance as good as possible by minimizing the mean-squared-error of each new pair of neurons in the topographic null model. Furthermore, we also respected, for each topographic null assembly, the proportion of neurons in either tectal hemisphere as observed in the original assembly. When the last iteration was performed, we only kept the topographic null model if the physical distance off all its pairs of neurons was not significantly different ($p > 0.05$) from the original assembly. The preservation of these properties enabled testing the specificity of the neuronal associations present in the assemblies. Assessing the significance of the different properties of the neuronal assemblies with respect to their null models enabled the comparison between experiments, independently of the variable number of tectal neurons found at the different developmental stages.

Compactness and Lateralization indexes
To assess the topographic dispersion of each assembly, we implemented a *compactness index* (*CI*), defined as:

$$CI = 1 - \frac{\sum_{i=1}^{n} d_i}{\left\langle \sum_{j=1}^{n} d_j \right\rangle}$$

The sum of the all distances of each neuron of an assembly to its centroid (d_i) was divided by the averaged sum of each neuron of the respective null-model assembly to their centroid (d_j). This allows taking into account the variable number of neuron in each

assembly, and compare within and between each condition.

We defined a *lateralization index* ranging from -1 to 1. One represents a neuronal assembly with all its neurons in a given hemisphere of the tectum, while the neurons of its corresponding null-model assemblies are equally present in both hemispheres. Reciprocally, -1 depicts a case where all the neurons of the null-model assemblies are in a given hemisphere, while neurons of the neuronal assembly are equally present in both hemispheres. Zero represents a neuronal assembly and its corresponding null model assemblies with the same proportion of neurons in a given hemisphere.

Normalization of the tectal anatomical coordinates

We transformed the position coordinates of the tectal neurons into a normalized reference space to compare topographical features across larvae of different developmental stages and in the intact and the enucleated conditions. The tectum possesses two clear morphological axes: the caudo-rostral axis and its perpendicular one, the medio-lateral axis (Figure S4A). We chose to project and normalize the coordinates of all imaged neurons with respect to these two axes. We first manually delineated the boundaries of the tectum, and used its midline and the border between the stratum periventricular and the neuropil to calculate the curve that best described the two axes. These axes were then normalized from -1 to 0, caudal to rostral for the left hemisphere, and 0 to 1, rostral to caudal, for the right one. Neurons from the left and right hemispheres of the tectum were projected into a [-1,0] x [-1,1] and [0,1]x[-1,1] normalized space respectively. Due to the curvature of the caudo-rostral axis, some neurons could be potentially equally mapped to two distinct normalized positions. In these rare cases, we chose to project the neuron over the axis position closest to its original position to solve this ambiguity.

Supplemental references

Brainard, D.H., 1997. The Psychophysics Toolbox. Spat. Vis. 10, 433–436.

Hilgetag, C., Kötter, R., Stephan, K., Sporns, O., 2002. Computational methods for the analysis of brain connectivity, in: Ascoli, G.A. (Ed.), Computational Neuroanatomy: Principles and Methods. Humana Press, pp. 295–336.

Lin, J., 1991. Divergence measures based on the Shannon entropy. Inf. Theory, IEEE Trans. 37, 145–151.

Lopes-dos-Santos, V., Ribeiro, S., Tort, A.B.L., 2013. Detecting cell assemblies in large neuronal populations. J. Neurosci. Methods 220, 149–166.

Peyrache, A., Benchenane, K., Khamassi, M., Wiener, S.I., Battaglia, F.P., 2010. Principal component analysis of ensemble recordings reveals cell assemblies at high temporal resolution. J. Comput. Neurosci. 29, 309–325.

Sporns, O., Honey, C.J., Kötter, R., 2007. Identification and classification of hubs in brain networks. PLoS One 2, e1049.